Cluster percolation and dynamical scaling in the Baxter-Wu model

Alexandros Vasilopoulos [ORCID],[1,*] Michail Akritidis [ORCID],[2,†] Nikolaos G. Fytas [ORCID],[1,‡] and Martin Weigel [ORCID][3,4,§]

[1]*School of Mathematics, Statistics and Actuarial Science, University of Essex, Colchester CO4 3SQ, United Kingdom*
[2]*Institut de Mathématiques de Bourgogne, Université de Bourgogne Europe, 21078 Dijon, France*
[3]*Institut für Physik, Technische Universität Chemnitz, 09107 Chemnitz, Germany*
[4]*Physics Department, Emory University, Atlanta, Georgia, USA*

We investigate the percolation behavior of Fortuin-Kasteleyn-type clusters in the spin-1/2 Baxter-Wu model with three-spin interactions on a triangular lattice. The considered clusters are constructed by randomly freezing one of the three sublattices, resulting in effective pairwise interactions among the remaining spins. Using Monte Carlo simulations combined with a finite-size scaling analysis, we determine the percolation temperature of these stochastic clusters and show that it coincides with the exact thermal critical point of the model. The critical exponents derived from cluster observables are consistent with those of the underlying thermal phase transition. Finally, we analyze the dynamical scaling of the multicluster and single-cluster algorithms resulting from the cluster construction, highlighting their efficiency and scaling behavior with system size.

I. INTRODUCTION

Cluster algorithms are a powerful tool for studying condensed-matter systems, particularly in the vicinity of continuous phase transitions [1]. Owing to the nonlocal nature of their update moves, they can substantially reduce—and in some cases practically eliminate—critical slowing down, which severely limits the efficiency of local Monte Carlo simulations in the presence of divergent spatial correlations. The archetypal, and spectacularly successful, examples are found in the Ising and Potts models which, as shown by Fortuin and Kasteleyn [2–4] and independently by Coniglio and Klein [5], admit a formulation in an extended space of spin and auxiliary bond variables, now known as the Fortuin-Kasteleyn-Coniglio-Klein (FKCK) representation. With the help of alternating updates in the spin and bond subspaces, Swendsen and Wang [6] and later Wolff [7] developed rejection-free cluster Monte Carlo algorithms that achieve a fundamental acceleration in the decorrelation of system configurations. The key to this success lies in the coincidence of the onset of percolation of FKCK clusters with the thermal phase transition of the spin model, as well as in the fact that the geometric properties of the critical clusters mirror the critical correlations of the spin degrees of freedom (for a recent review, see Ref. [8]).

These algorithms work extremely well for the Potts model. Based on the embedded-cluster trick proposed by Wolff [7], extensions to continuous-spin models with analogous interactions are straightforward and similarly effective. When moving beyond these paradigmatic examples, however, cluster approaches often become more difficult to construct and/or do not work so well. Although somewhat more general cluster-update frameworks have been proposed [9–11], they do not yield efficient algorithms in all situations, in particular, for systems with frustrated interactions. (Even greater challenges arise in the presence of additional disorder; see Ref. [12].) An especially interesting case occurs for systems with multispin interactions, where an extension of configuration space in terms of bond variables is no longer particularly natural. Such models appear in several contexts, including proposals for quantum computing architectures [13,14], the design of alternative storage devices [15], models exhibiting glassy dynamics without quenched disorder [16], and studies of metastable phases following quenches [17].

The simplest nontrivial example of such a system is the Baxter-Wu (BW) model, an Ising model on the triangular lattice with three-spin interactions [18]. While, in principle, a cluster algorithm based on freezing triangular plaquettes could be devised following the general framework of Refs. [10,11], the only concrete proposal to date for the Baxter-Wu model is due to Novotny and Evertz [19]. Their approach effectively reduces the problem to the case of pairwise interactions by freezing one of the three sublattices of the triangular lattice and constructing clusters on the remaining two. Building upon this idea, Deng *et al.* [20] developed cluster-update schemes for generalized variants of the problem, including versions with two distinct interaction strengths and others incorporating three-spin interactions in a q-state Potts model. To date, however, a detailed analysis of the approach of Novotny and Evertz has not been presented. (Ref. [21] largely repeats the original construction using different terminology,

---
*Contact author: alex.vasilopoulos@essex.ac.uk
†Contact author: michalis.akritidis@u-bourgogne.fr
‡Contact author: nikolaos.fytas@essex.ac.uk
§Contact author: martin.weigel@physik.tu-chemnitz.de

without offering significant further insight). It has also been argued that the resulting clusters may not percolate precisely at the thermal critical point [22], a phenomenon observed in several related systems [23–25]. In other words, the percolation threshold of the constructed clusters, T_p, may differ from the actual critical temperature, T_c, implying that, asymptotically, the stochastic spin clusters cannot serve to efficiently decorrelate configurations as the system size increases.

Hence, a detailed percolation analysis of the original cluster construction introduced in Ref. [19] has so far been lacking in the literature. In the present work, we close this gap in the understanding of cluster updates for spin systems by performing a comprehensive study of the percolation properties of the Novotny-Evertz clusters for the Baxter-Wu model. We find that these clusters indeed percolate precisely at the thermal critical point and fully capture the thermal critical behavior, thereby providing a firm justification for constructing cluster algorithms based on this prescription. By investigating both multicluster and single-cluster variants, we further demonstrate that these algorithms significantly reduce autocorrelation times compared to single-spin flip updates, and we determine the corresponding dynamical critical exponents.

The rest of this paper is organized as follows. In Sec. II, we introduce the Baxter-Wu model, describe the Monte Carlo algorithms employed in our simulations, and define the observables used in both the cluster and dynamical analyses. Section III contains our main results. Specifically, Sec. III A focuses on determining the percolation threshold of the clusters and extracting the associated critical exponents, while Sec. III B provides a detailed analysis of the dynamical scaling behavior of the algorithm at equilibrium as a function of system size. Finally, Sec. IV summarizes our main findings and outlines potential directions for future work.

II. MODEL AND NUMERICS

A. Model

We consider the spin-1/2 BW model, defined on a triangular lattice by the Hamiltonian [18]

$$\mathcal{H} = -J \sum_{\langle ijk \rangle} \sigma_i \sigma_j \sigma_k, \qquad (1)$$

where the Ising spins σ_i take values ± 1, and the summation extends over all elementary triangular plaquettes formed by nearest-neighbor triplets $\langle ijk \rangle$. Throughout this work, we set the interaction strength $J = 1$, thereby fixing the energy scale, and we apply periodic boundary conditions. As illustrated in Fig. 1, the triangular lattice decomposes naturally into three interpenetrating sublattices (A, B, and C), such that each corner of a triangle belongs to a different sublattice. For a system of linear size L, each sublattice contains $N/3$ spins, where $N = L^2$ is the total number of lattice sites.

The characteristic three-spin interaction results in a loss of the overall spin-inversion symmetry of the standard Ising model. On the other hand, a simultaneous inversion of all spins on any two sublattices leaves the Hamiltonian invariant, resulting in a fourfold degenerate ground state. Originally introduced by Wood and Griffiths as a variation of the Ising model with three-spin interactions that preserves self-duality
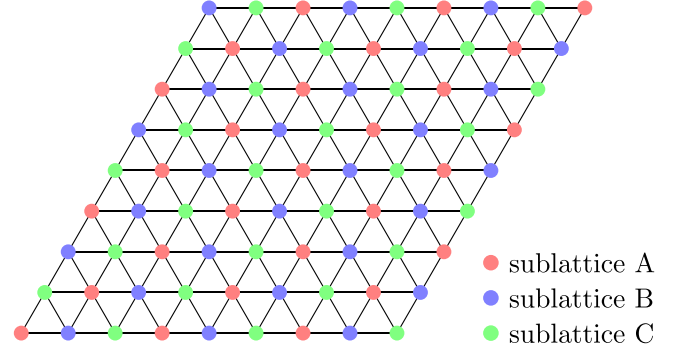

FIG. 1. Example of a 9×9 triangular lattice with the three sublattices distinguished by color. Each spin interacts with its nearest neighbors on the other two sublattices, illustrating the triplet-interaction structure characteristic of the BW model.

[18], the BW model was later solved exactly by Baxter and Wu [26–29]. It was shown to belong to the same universality class as the four-state Potts model, exhibiting a continuous phase transition with central charge $c = 1$ (but without logarithmic corrections).

B. Algorithms

For constructing stochastic clusters, we follow the original proposal of Novotny and Evertz [19]. Their approach starts from the observation that we know how to construct cluster updates for standard Ising systems through the FKCK representation. They hence suggested a transformation of the BW model into an effective two-body problem achieved by freezing all spins on one of the three sublattices (which is randomly selected at each update step). As a result, the spins on the remaining two sublattices acquire effective two-body couplings given by

$$J'_{ij} = J(\sigma_{\perp(i,j),+1} + \sigma_{\perp(i,j),-1}), \qquad (2)$$

where $\sigma_{\perp(i,j),\pm1}$ denote the two spins on the frozen sublattice opposite of the bond (i, j).

An example of this construction is illustrated in Fig. 2, where sublattice C is frozen, resulting in renormalized couplings between the A spin σ_0 and the B spins σ_2, σ_4,
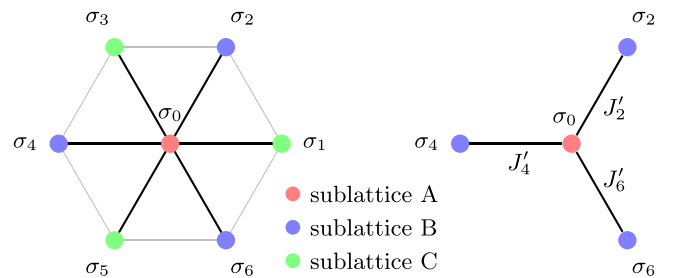

FIG. 2. Local mapping of the triangular lattice onto a honeycomb lattice by freezing one of the three sublattices. In the example shown, the spins on the frozen C sublattice lead to effective pair interactions between the spins on the A and B sublattices, denoted by J'. For the bond $(0, 2)$, the opposite spins on sublattice C are $\sigma_{\perp(0,2),+1} = \sigma_3$ and $\sigma_{\perp(0,2),-1} = \sigma_1$.

and σ_6. We note that the frozen sublattice and the resulting honeycomb lattice are dual to each other. Since we set $J = 1$ throughout, the effective couplings J'_{ij} take values in $\{-2, 0, +2\}$, corresponding to antiferromagnetic, diluted, and ferromagnetic bonds, respectively. Importantly, this procedure introduces no frustration: the product of the couplings along any hexagon, and hence around any closed loop, is nonnegative.

As a consequence, the resulting effective Ising model with only pairwise interactions on a diluted honeycomb lattice can be simulated using standard FKCK-based cluster algorithms. The established proof of detailed balance for these algorithms for the conventional Ising and Potts models therefore applies directly here. Moreover, because the choice of the frozen sublattice is random, the dynamics are ergodic (the probability of all clusters consisting of a single spin is nonzero) and hence must converge to the correct equilibrium distribution according to the Markov theorem [19].

If a spin σ_i already belongs to a given cluster, a neighboring spin σ_j is eligible to be added to the cluster if the effective interaction is satisfied, i.e., if $J'_{ij}\sigma_i\sigma_j > 0$. Following the FKCK rules, the probability of adding such a spin is given by

$$p_{\text{add}} = 1 - \exp\left(-2|J'_{ij}|/T\right),$$

where T is the system temperature. Bonds with $J'_{ij} = 0$ can be retained without explicitly considering a diluted lattice, as they will never be activated. A simplified multicluster implementation (in the spirit of the Swendsen–Wang algorithm) proceeds as follows:

(1) Randomly freeze one sublattice (e.g., sublattice C, as shown in Fig. 2). Only spins on the remaining two sublattices are considered for the cluster construction.

(2) Choose a seed spin that has not yet been assigned to a cluster.

(3) For each of its three neighbors not already in a cluster, check whether the effective interaction condition $J'_{ij}\sigma_i\sigma_j > 0$ is satisfied. If so, add the neighbor to the current cluster with probability $p_{\text{add}} = 1 - \exp(-4/T)$.

(4) Continue growing the cluster recursively by applying step 3 to newly added spins until no further spins can be added.

(5) If any unassigned spins remain, return to step 2.

(6) Once all $2N/3$ active spins have been assigned to clusters, flip each cluster with probability $1/2$. Return to step 1 for the next Monte Carlo step.

A single-cluster update (analogous to the Wolff algorithm) can be implemented by constructing a single cluster per Monte Carlo step, initiated from a randomly chosen spin in one of the active sublattices. Each spin may participate in only one cluster per step. Depending on the signs of the effective interactions, the resulting clusters can be ferromagnetic or antiferromagnetic. However, due to the bipartite nature of the honeycomb lattice, the fixed configuration of the frozen sublattice, and the available spin values, clusters containing both ferromagnetic and antiferromagnetic bonds are not possible.

In a single Monte Carlo step, $2N/3$ spins—those not on the frozen sublattice—are considered for updates, thereby defining one Monte Carlo time step for the multicluster update. It is clear from the construction of the system that for the sublattice decomposition, and hence the validity of the presented
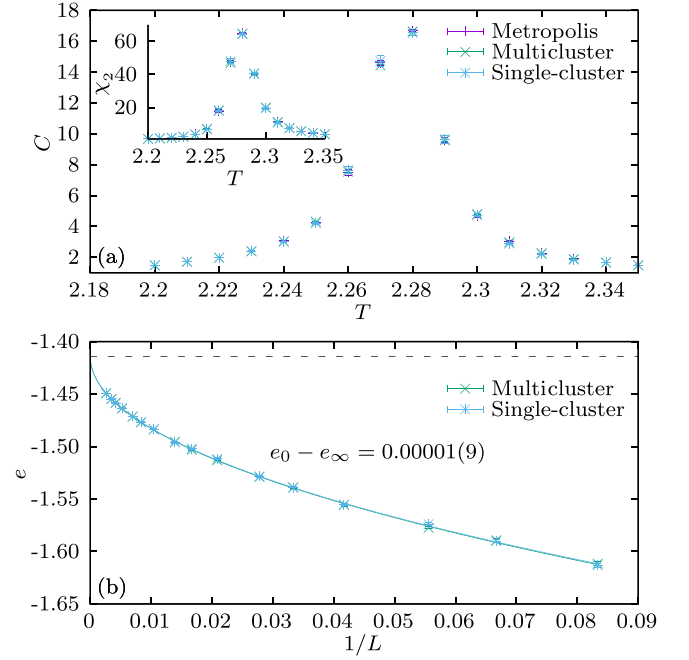

FIG. 3. (a) Comparison of simulation results obtained using the Metropolis, single-cluster, and multicluster updates for the specific heat and magnetic susceptibility of the spin-1/2 BW model at various temperatures for a system of linear size $L = 48$. The main panel shows the specific heat $C(T)$, while the inset displays the magnetic susceptibility $\chi_2(T)$. The excellent agreement between the methods confirms the correctness of the cluster-algorithm implementation. (b) Finite-size scaling of the energy at the critical point. The exact result $e_0 = -\sqrt{2}$ [26–28] is indicated by the dashed line.

algorithms, L and $N = L^2$ must be multiples of three. The correctness of the cluster-update scheme and our implementation was ascertained, among other checks, by comparing various quantities between the Metropolis and cluster simulations. The result of such comparisons are summarized in Fig. 3. In particular, Fig. 3(a) shows a the specific heat C [main panel, Eq. (7)] and the magnetic susceptibility χ_2 [inset, Eq. (10)] obtained using the multi- and single-cluster algorithms as well as results from the standard Metropolis algorithm [1,30] for a system of linear size $L = 48$. All data are fully compatible within statistical errors. Figure 3(b) illustrates the finite-size scaling (FSS) behavior of the energy and its convergence toward the exact asymptotic value $e_0 = -\sqrt{2}$ [26–28] for the two cluster algorithms. Since the multicluster and single-cluster simiuations are statistically independent, we perform a joint fit to the two data sets using the ansatz [31]

$$e(L) = e_\infty + bL^{-(d-1/\nu)},$$

where e_∞ denotes the thermodynamic-limit value of the energy, b is a fitting parameter, $d = 2$ is the spatial dimensionality, and $\nu = 2/3$ corresponds to the Baxter-Wu universality class. Allowing both e_∞ and $d - 1/\nu$ to vary, we obtain $e_0 - e_\infty = 0.0002(4)$ and $d - 1/\nu = 0.502(4)$. Fixing $d - 1/\nu = 0.5$ and refitting yields $e_0 - e_\infty = 0.00001(9)$. Finally, fixing $e_\infty = -\sqrt{2}$ and fitting only the remaining parameters gives $d - 1/\nu = 0.5000(8)$. All results are in excellent agreement with the expected values.

In our production runs, we performed 10^5 Monte Carlo steps for sampling at the smallest system size, $L = 12$, with an additional 10^4 steps used for equilibration. For larger systems, the number of Monte Carlo steps was scaled proportionally to $N/12^2$, roughly accounting for the expected dynamical critical exponent $z \approx 2$ for local algorithms. Specifically, we considered systems with linear sizes $12 \leqslant L \leqslant 384$. For each size, 20 independent realizations were simulated, and statistical analysis was performed using the jackknife method [32]. Critical behavior was extracted via least-squares fitting, with a lower cutoff $L \geqslant L_{\min}$ chosen to account for scaling corrections. Fit quality was assessed using the standard χ^2 test [33], and fits were deemed acceptable if the goodness-of-fit parameter satisfied $Q \geqslant 10\%$ [33].

C. Observables

While the discussion above demonstrates that the proposed cluster update is formally correct, it is not *a priori* clear whether it is effective in alleviating critical slowing down. One necessary condition is that the clusters just begin to percolate at the point of the thermal phase transition; otherwise, they will asymptotically include either very few or nearly all spins, effectively reducing the update to a local move. To investigate the percolation properties of the BW clusters introduced above, we studied standard observables from percolation theory [34], namely, the wrapping probability P_{wrap}, the average cluster size S, and the percolation strength P_{∞}.

The wrapping (or spanning) probability P_{wrap} is defined as the probability that at least one cluster spans the periodic boundaries of the system, wrapping around the lattice and reconnecting with itself. In the thermodynamic limit, the wrapping probability P_{wrap} becomes a discontinuous function of temperature, taking the value $P_{\mathrm{wrap}} = 0$ above the percolation transition temperature T_{p} and $P_{\mathrm{wrap}} = 1$ below it. This discontinuity signals the appearance of percolating clusters for $T < T_{\mathrm{p}}$. In contrast, for finite systems, $P_{\mathrm{wrap}}(T)$ is a smooth, continuous function. Nonetheless, curves corresponding to different system sizes are expected to intersect at a common point—modulo finite-size effects—marking the percolation transition. Depending on the spatial direction in which clusters wrap, various definitions of P_{wrap} can be employed [35–37]. In this study, a cluster is considered to percolate if it wraps around and reconnects to itself in either the horizontal or vertical direction, or in both directions. As a dimensionless quantity, P_{wrap} is expected to obey the standard FSS form [34]

$$P_{\mathrm{wrap}}(t, L) = \tilde{P}_{\mathrm{wrap}}(tL^{1/\nu}), \tag{3}$$

where $\tilde{P}_{\mathrm{wrap}}$ is a universal scaling function, $t = (T - T_{\mathrm{p}})/T_{\mathrm{p}}$ is the reduced temperature, and ν is the critical exponent associated with the divergence of the correlation length.

The average cluster size is defined as

$$S = \frac{\sum_s n_s s^2}{\sum_s n_s s}, \tag{4}$$

where n_s denotes the number of clusters of size s [34]. In the thermodynamic limit, excluding the (infinite) percolating cluster from the sums in Eq. (4) causes S to peak near the percolation transition. This intermediate maximum arises because at high temperatures the system consists predominantly of small clusters, whereas below the percolation threshold T_{p} most spins belong to the macroscopic percolating cluster (which is excluded from the sums). To reproduce this behavior in finite systems, the largest cluster is excluded from each measurement. As a result, S develops a peak at a pseudocritical temperature, which approaches T_{p} as the system size increases. In the critical regime, S obeys the FSS form

$$S(t, L) = L^{\gamma/\nu}\tilde{S}(tL^{1/\nu}), \tag{5}$$

where γ/ν is the ratio of critical exponents associated with the divergence of the average cluster size, analogous to the finite-size scaling exponent of the magnetic susceptibility [34]. In previous numerical studies, it was noted that this exclusion of percolating clusters (or an analogous subtraction in the susceptibility) introduces significant scaling corrections in Ising-like systems [37,38]. In the present work, we therefore use a definition of S that includes all clusters, without omitting the largest or spanning clusters. The downside of this approach, of course, is that S no longer exhibits a maximum, and must instead be evaluated either at the fixed temperature T_{p} or at a separately determined sequence of pseudocritical points.

The percolation strength P_{∞} denotes the probability that a randomly selected spin belongs to the percolating cluster. It is computed as the fraction of sites comprising the largest, system-spanning cluster. In the thermodynamic limit, $P_{\infty} = 0$ above the percolation threshold, indicating the absence of a spanning cluster, while below T_{p} it grows continuously, approaching $P_{\infty} = 1$ as $T \to 0$, where all spins belong to a single connected cluster. Serving as an order parameter—analogous to the magnetization in a thermal phase transition—P_{∞} captures the onset of long-range connectivity. Its FSS form is given by [34]

$$P_{\infty}(t, L) = L^{-\beta/\nu}\tilde{P}_{\infty}(tL^{1/\nu}), \tag{6}$$

where β/ν is the finite-size scaling exponent associated with the order parameter.

To study the thermodynamic properties of the system and, by extension, the dynamical properties of the algorithm, we measured the internal energy E, from which the specific heat is obtained via the standard fluctuation–dissipation relation as

$$C = (\langle E^2 \rangle - \langle E \rangle^2)/(NT^2). \tag{7}$$

Magnetic ordering was characterized by evaluating the magnetization on each of the three sublattices, denoted by M_{A}, M_{B}, and M_{C}. From these, we define two commonly used order parameters:

$$m_1 = (|m_{\mathrm{A}}| + |m_{\mathrm{B}}| + |m_{\mathrm{C}}|)/3, \tag{8}$$

$$m_2 = \sqrt{\left(m_{\mathrm{A}}^2 + m_{\mathrm{B}}^2 + m_{\mathrm{C}}^2\right)\big/3}, \tag{9}$$

where $m_x = M_x/(N/3)$ for each sublattice $x = \mathrm{A}$, B, and C [39–41]. In the thermodynamic limit, both m_1 and m_2 approach unity in the fully ordered ground states and vanish in the completely disordered (paramagnetic) state. The associated magnetic susceptibilities are defined as

$$\chi_i = \frac{N\left(\langle m_i^2 \rangle - \langle m_i \rangle^2\right)}{T}, \quad i = 1, 2, \tag{10}$$
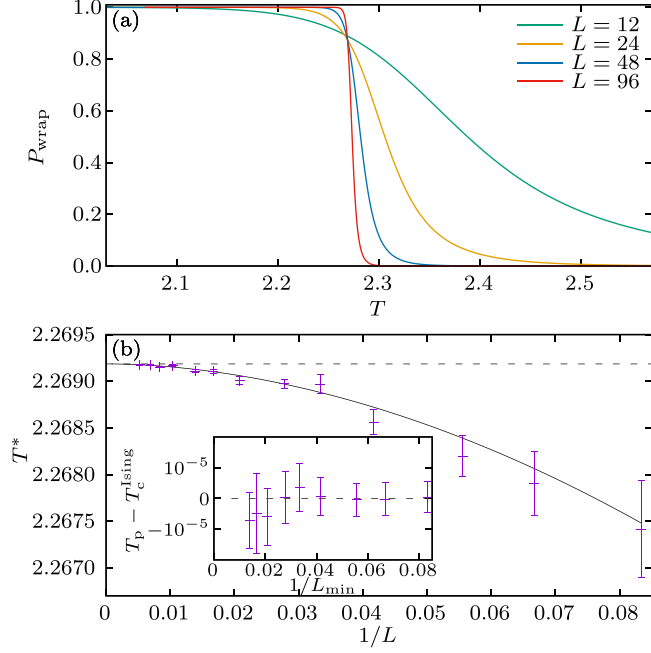
FIG. 4. (a) Wrapping probability as a function of temperature for different system sizes. (b) Extrapolation of the percolation temperature T_p from the crossings of the wrapping probability curves according to Eq. (12). The horizontal dashed line indicates the exact critical temperature T_c of the BW model. The inset shows the difference $T_p - T_c$ as a function of the minimum system size L_{min} included in the fits. The excellent agreement between the two temperatures supports identifying the percolation transition with the thermal phase transition.

quantifying the fluctuations in the respective order parameters.

As shown by Wood and Griffiths [18], the BW model is self-dual and consequently exhibits the same critical temperature as the regular square-lattice Ising model [29,42]:

$$T_c^{Ising} = \frac{2}{\ln(\sqrt{2}+1)} \approx 2.269\,185\,314\cdots. \tag{11}$$

All simulations were therefore conducted directly at this critical temperature. Furthermore, the use of the single-histogram reweighting technique [43] enabled efficient extraction of observables over a range of temperatures near criticality. Our independent estimate of the percolation temperature, reported below, additionally justifies this choice of simulation temperature *a posteriori*, confirming the self-consistency of the analysis.

III. RESULTS

A. Percolation analysis

To determine the percolation temperature, we analyzed the wrapping probabilities for pairs of system sizes $(L, 2L)$. As shown in Fig. 4(a), the wrapping probabilities approximately cross at a common point. According to standard arguments of FSS, these crossing points are expected to follow the law [31]

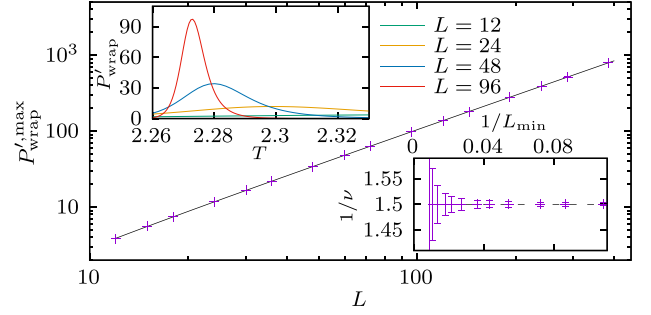$$T^*(L) = T_p + c_p L^{-(\omega+1/\nu)}, \tag{12}$$

FIG. 5. FSS of the derivatives of the wrapping probability evaluated at their respective maxima (main panel). The inset in the top left shows the temperature dependence of the derivative of the wrapping probability for several system sizes. The bottom-right inset displays the estimated exponent $1/\nu$ as a function of $1/L_{min}$ for fits including corrections and a free ω parameter; the horizontal dashed line marks the exact value $1/\nu = 3/2$.

where $T^*(L)$ denotes the crossing temperature, T_p is the percolation temperature in the thermodynamic limit $L \to \infty$, c_p is a nonuniversal amplitude, and ω is the correction-to-scaling exponent [44,45]. Figure 4(b) shows T^* as a function of $1/L$, while the inset displays the difference $T_p - T_c^{Ising}$ as a function of the minimum system size L_{min} included in the fits. From this analysis, we obtain the final estimate

$$T_p = 2.269\,186(5), \tag{13}$$

corresponding to $T_p - T_c^{Ising} = (0 \pm 5) \times 10^{-6}$, where we used $L_{min} = 12$ and the resulting exponent estimate is $\omega + 1/\nu = 1.9(1)$. (We will come back to this estimate further below in the present section.) Within numerical uncertainty, these results demonstrate that the percolation temperature of the clusters coincides with the critical temperature of the model.

The derivative of the wrapping probability is also of interest, as it provides an independent route to estimating the critical exponent ν. It was computed using a three-point numerical differentiation scheme based on histogram reweighting [43] with a temperature step of 10^{-6}. The peak value of this derivative is expected to follow the FSS relation [34]

$$P'^{,max}_{wrap}(L) = c_{P'} L^{1/\nu}(1 + d_{P'} L^{-\omega}), \tag{14}$$

where $c_{P'}$ and $d_{P'}$ are nonuniversal fitting constants, and the superscript "max" indicates evaluation at the maximum of P'_{wrap}. Figure 5 shows representative fits according to Eq. (14). Three types of fits were performed: (i) without corrections, excluding small system sizes to mitigate finite-size effects; (ii) including corrections with a fixed $\omega = 2$ [44,45]; and (iii) allowing ω to vary freely. For the first case, excluding the correction term, the estimates for $1/\nu$ are several standard deviations away from the expected value of $3/2$; for example, when $L_{min} = 120$, $1/\nu = 1.507(4)$. Only for $L_{min} \geq 192$ do we get values consistent with $3/2$: for $L_{min} = 192$ specifically, $1/\nu = 1.504(6)$. From the fits with a correction-to-scaling exponent set to $\omega = 2$, fits become acceptable for $L_{min} \geq 36$ and we again see a discrepancy from the exact value. Starting from $L_{min} \geq 120$, we find values in agreement with the expected

one: For example, with $L_{\min} = 120$, we find $1/\nu = 1.500(4)$. Interestingly, for all values of $L_{\min}$, corrections seem to remain relevant, since $d_{P'}$ does not disappear within errors, which would be expected as one eliminates smaller systems. With a free correction exponent, $1/\nu = 1.500(2)$ and $\omega = 1.0(2)$ for $L_{\min} = 12$. Importantly, despite the uncertainty in corrections, the estimates of $1/\nu$ remain consistent across all fitting procedures.

In view of the above results, one may wonder about the consistency of values of the correction-to-scaling exponent ω obtained from Eqs. (12) and (14). From the fit to the crossing temperatures [Eq. (12)], we find $\omega + 1/\nu = 1.9(1)$. Using any of our estimates of $1/\nu$, this corresponds to $\omega \approx 0.4$. However, previous studies by Alcaraz and Xavier [44,45] reported $\omega = 2$. On the other hand, the above quoted fit for $P'^{,\max}_{\mathrm{wrap}}(L)$ yields $\omega = 1.0(2)$, while we do not find evidence in favor of $\omega = 2$ in our data. These discrepancies suggest that the present data set may not be sufficient to reliably resolve subleading corrections to scaling, indicating that additional correction terms are likely relevant but cannot be captured within our accessible range of system sizes. Consequently, in the remainder of the analysis, we focus on fits including the correction exponent as a free parameter. Only when the constants in front of the correction term $L^{-\omega}$ become minuscule do we consider additional fitting processes.

Finally, by analyzing the scaling behavior of the percolation strength P_∞ and the average cluster size S, both evaluated at the critical temperature T_c of Eq. (11)—which according to our results equals the percolation temperature T_p—we obtain estimates for the critical exponent ratios β/ν and γ/ν. These quantities are expected to follow the FSS relations [34]

$$P^{T_c}_\infty(L) = c_P L^{-\beta/\nu}(1 + d_P L^{-\omega}), \qquad (15)$$

$$S^{T_c}(L) = c_S L^{\gamma/\nu}(1 + d_S L^{-\omega}), \qquad (16)$$

where c_P, c_S and d_P, d_S are nonuniversal fitting constants. The corresponding fits are shown in Figs. 6(a) and 6(b) for $P^{T_c}_\infty$ and S^{T_c}, respectively. As discussed in Sec. II C, our definition of S includes all clusters; consequently, this quantity does not exhibit a peak as a function of temperature. From the fits to Eqs. (15) and (16), we obtain $\beta/\nu = 0.1251(9)$ and $\gamma/\nu = 1.750(2)$, with $L_{\min} = 12$, both in excellent agreement with the exact values $\beta/\nu = 1/8$ and $\gamma/\nu = 7/4$ characteristic of the BW universality class. The corresponding corrections-to-scaling exponents are $\omega = 1.3(8)$ and $1.0(3)$. For the β/ν fits, the correction amplitude d_P is consistently zero within errors. Fits performed without corrections yield compatible results for $L_{\min} \geqslant 120$ only; for example, $\beta/\nu = 0.1244(6)$, $0.1243(7)$, $0.124(1)$, $0.123(1)$ for $L_{\min} = 120, 144, 192, 240$, respectively, all consistent with the expected value $1/8$.

B. Dynamical critical exponent

To estimate the dynamical critical exponent z of the cluster algorithms, we first compute the integrated autocorrelation times τ for three observables: the energy [Eq. (1)] and the two order parameters defined in Eqs. (8) and (9). The corresponding autocorrelation times, denoted as τ_e, τ_{m_1}, and τ_{m_2}, are evaluated at the critical temperature. Their scaling behavior
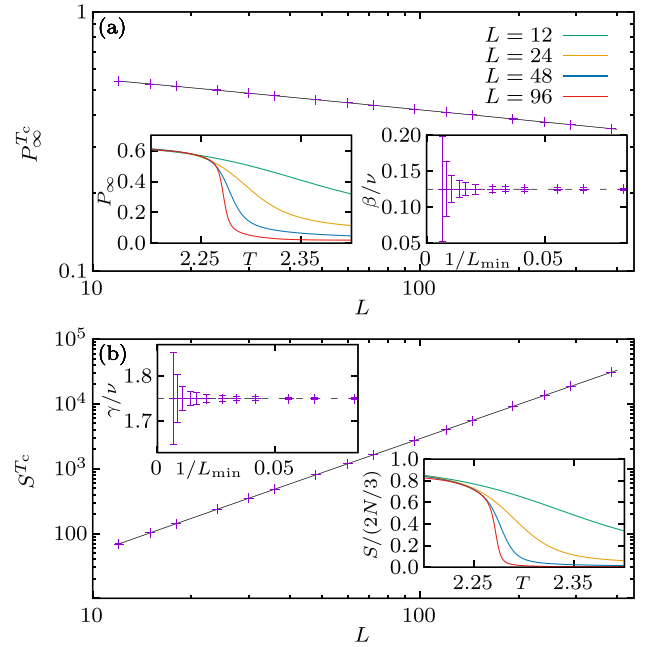

FIG. 6. FSS of (a) the percolation strength P_∞ and (b) the average cluster size S, including the largest cluster. Both observables are evaluated at the Ising-model critical temperature (11). Power-law fits yield the critical exponent ratios β/ν and γ/ν, respectively. The insets show the estimated exponents as a function of $L_{\min}$, with horizontal dashed lines indicating the exact values $\beta/\nu = 1/8$ and $\gamma/\nu = 7/4$. Also included are insets with the corresponding curves of P_∞ and the normalized cluster size $S/(2N/3)$.

with system size is expected to follow the FSS ansatz [46]

$$\tau_x(L) = c_x L^{z_x}(1 + d_x L^{-\omega}), \qquad (17)$$

where c_x and d_x are nonuniversal fitting coefficients, and $z_x \equiv z^{\mathrm{int}}_x$ denotes the (integrated) dynamical critical exponent associated with observable $x \in \{e, m_1, m_2\}$. We note that the observable-independent exponent $z^{\exp}$, which characterizes the scaling of exponential autocorrelation times, is not considered in the present analysis.

The integrated autocorrelation times τ_x are defined via a summation of the normalized autocorrelation functions,

$$A_x(t') = \frac{\langle x(t)x(t+t')\rangle - \langle x(t)\rangle\langle x(t+t')\rangle}{\langle x(t)^2\rangle - \langle x(t)\rangle^2}, \qquad (18)$$

where x denotes the observable under consideration. In practice, the natural estimator $\hat{A}_x(t')$ of the autocorrelation function is computed directly from the time series of measurements. The integrated autocorrelation time is then estimated employing a summation cutoff [47–49]:

$$\hat{\tau}_x = I_x(k^{(x)}_{\max}) = \frac{1}{2} + \sum_{t'=1}^{k^{(x)}_{\max}} \hat{A}_x(t'). \qquad (19)$$

The cutoff $k^{(x)}_{\max}$ is determined self-consistently as the smallest lag t' satisfying $k^{(x)}_{\max} > 6\hat{\tau}_x$ [47]. This criterion provides a useful tradeoff between the systematic error for too small cutoff $k^{(x)}_{\max}$ and a divergent variance of the estimator for $k^{(x)}_{\max} \to \infty$. For the single-cluster algorithm, the definition of one Monte Carlo time step must take into account that only a
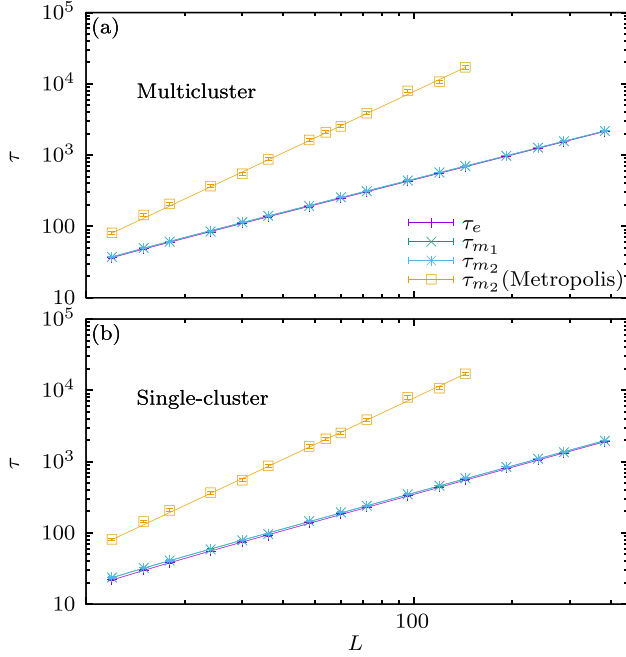
FIG. 7. Scaling behavior of the integrated autocorrelation times for the energy and the two order parameters defined in Eqs. (8) and (9). The dynamical critical exponent z is extracted via fits of the scaling form in Eq. (17). Panel (a) shows results for the multicluster update, while (b) corresponds to the single-cluster update. For comparison, Metropolis results for m_2 are also included. All curves exhibit an overall linear trend on a log-log scale, with the single-cluster data displaying a slightly steeper slope than the multicluster results.

TABLE I. Final estimates of the dynamical critical exponent z of the integrated autocorrelation times for the multi- and single-cluster algorithms (labeled MC and SC, respectively) in the BW model, based on the three observables analyzed in this work. We show results obtained with fixed corrections using $\omega = 2$, with free corrections with variable ω, and without scaling corrections [see Eq. (17)]. For comparison, the last two rows include the estimate from Ref. [19] and our results obtained using the Metropolis algorithm.

Algorithm	Fit type	z_e	z_{m_1}	z_{m_2}
	Free correction	1.157(15)	1.152(15)	1.152(15)
MC	Fixed correction	1.163(3)	1.158(3)	1.159(3)
	No correction	1.166(3)	1.161(3)	1.162(3)
	Free correction	1.254(22)	1.246(22)	1.246(22)
SC	Fixed correction	1.255(6)	1.247(6)	1.247(6)
	No correction	1.257(5)	1.248(5)	1.248(5)
Ref. [19]	No correction			1.37(10)
Metropolis	No correction			2.16(3)

single cluster is constructed per update. To ensure comparable time units with the multicluster algorithm, we scale time by a factor $\langle C \rangle/(2N/3)$, corresponding to the average fraction of the $2N/3$ active sites at each step that is updated in one single-cluster step with average cluster size $\langle C \rangle$. This normalization allows for a direct comparison of autocorrelation times between the two update schemes.

Our main results for the autocorrelation times of the cluster updates are presented in Fig. 7, which also shows, for comparison, the autocorrelation behavior of the m_2 observable calculated with the Metropolis algorithm. The dynamical critical exponent z is extracted by fitting the system-size dependence of the integrated autocorrelation times τ_x to the FSS form given in Eq. (17). The resulting estimates for the single- and multicluster algorithms are summarized in Table I. For fits with a free corrections-to-scaling exponent ω, the terms d_x consistently vanish for all x, for both the single- and the multicluster algorithm. However, when ω is fixed to 2 [44,45], we find a nonzero amplitude if using small L_{min}. In these cases including corrections, the results stated in Table I are for $L_{min} = 12$. For the case without corrections, L_{min} is 24 for the multicluster and 48 for the single-cluster case. Similar to the results in Sec. III A, our estimates of z are consistent regardless of the method used and across all observables. From the fits without corrections to scaling, we obtain average estimates of $z = 1.162(3)$ for the multicluster update [Fig. 7(a)] and $z = 1.251(5)$ for the single-cluster update [Fig. 7(b)]. The latter

lies at the lower end of the estimate reported by Novotny and Evertz, $z = 1.37(10)$ [19], which was obtained using a single-cluster implementation and based on the root-mean-square sublattice magnetization [see Eq. (9)]. Both cluster algorithms clearly outperform the Metropolis method, for which we find $z = 2.16(3)$, demonstrating a substantial reduction of critical slowing down. The Metropolis result is, within statistical uncertainty, consistent with that of the Ising model [50–52].

IV. CONCLUSIONS

We have investigated the percolation properties of clusters in the spin-1/2 Baxter-Wu model using the construction scheme proposed by Novotny and Evertz [19], in which one sublattice is frozen and clusters are built on the remaining two. Implementing a multicluster update within this framework, we first verified that, within numerical accuracy, the clusters percolate precisely at the known critical temperature of the model. Furthermore, we extracted the critical exponent ratios $1/\nu$, β/ν, and γ/ν associated with the cluster observables and found them to be consistent with the known thermal values of the universality class. These findings confirm the validity of the algorithm and its suitability for simulating the Baxter-Wu model.

To assess the efficiency of the cluster algorithm, we analyzed its dynamical critical behavior by estimating the exponent z from the scaling of integrated autocorrelation times for various observables, considering both multi- and single-cluster implementations. The integrated autocorrelation time was computed using a self-consistent cutoff method. This analysis yields estimates of $z = 1.251(5)$ for the single-cluster variant and $z = 1.162(3)$ for the multicluster algorithm. These values lie close to the lower bound imposed by the Li-Sokal inequality, $z \geqslant \alpha/\nu = 2/\nu - d = 1$ [53], indicating that these cluster algorithms operate near optimal efficiency for the Baxter-Wu model.

Our present study lays the groundwork for a similar percolation and dynamical scaling analysis in the spin-1 generalization of the Baxter-Wu model, which includes a

chemical potential [54–57]. In this setting, the presence of zero spins may hinder the effectiveness of cluster algorithms, particularly at larger crystal-field strengths Δ, where the density of zero spins increases significantly. Interestingly, this model allows for clusters that combine both ferromagnetic and antiferromagnetic interactions. Since zero spins cannot be easily included in the cluster construction, a pure cluster algorithm is no longer ergodic and must be complemented by local single-spin updates in a hybrid scheme—a strategy that has proven successful for other spin-1 models [58]. This generalized model is also believed to host a pentacritical point [54–57], leading to a phase diagram containing both first- and second-order transition lines. This raises several intriguing questions: (i) Do the clusters still percolate at the transition points? (ii) How does the dynamical critical exponent z behave near the putative multicritical point? (iii) Does z depend systematically on Δ?

Another promising avenue is the study of the gonihedric Ising model [59,60], where the presence of plaquette interactions complicates cluster construction. In this case, a modified cluster approach—splitting the lattice into frozen and active sublattices to induce effective interactions—may provide a viable strategy for future investigations.

DATA AVAILABILITY

The data that support the findings of this article are not publicly available upon publication because it is not technically feasible and/or the cost of preparing, depositing, and hosting the data would be prohibitive within the terms of this research project. The data are available from the authors upon reasonable request.

[1] D. P. Landau and K. Binder, *A Guide to Monte Carlo Simulations in Statistical Physics*, 5th ed. (Cambridge University Press, Cambridge, 2021).

[2] C. Fortuin and P. Kasteleyn, On the random-cluster model: I. Introduction and relation to other models, Physica **57**, 536 (1972).

[3] C. Fortuin, On the random-cluster model II. The percolation model, Physica **58**, 393 (1972).

[4] C. Fortuin, On the random-cluster model: III. The simple random-cluster model, Physica **59**, 545 (1972).

[5] A. Coniglio and W. Klein, Clusters and Ising critical droplets: A renormalisation group approach, J. Phys. A **13**, 2775 (1980).

[6] R. H. Swendsen and J.-S. Wang, Nonuniversal critical dynamics in Monte Carlo simulations, Phys. Rev. Lett. **58**, 86 (1987).

[7] U. Wolff, Collective Monte Carlo updating for spin systems, Phys. Rev. Lett. **62**, 361 (1989).

[8] A. Coniglio and A. Fierro, Correlated percolation, in *Complex Media and Percolation Theory*, edited by M. Sahimi and A. G. Hunt (Springer, New York, 2021), p. 61.

[9] R. G. Edwards and A. D. Sokal, Generalization of the Fortuin-Kasteleyn-Swendsen-Wang representation and Monte Carlo algorithm, Phys. Rev. D **38**, 2009 (1988).

[10] D. Kandel, R. Ben-Av, and E. Domany, Cluster dynamics for fully frustrated systems, Phys. Rev. Lett. **65**, 941 (1990).

[11] D. Kandel and E. Domany, General cluster Monte Carlo dynamics, Phys. Rev. B **43**, 8539 (1991).

[12] L. Münster and M. Weigel, Cluster percolation in the two-dimensional Ising spin glass, Phys. Rev. E **107**, 054103 (2023).

[13] J. K. Pachos and M. B. Plenio, Three-spin interactions in optical lattices and criticality in cluster Hamiltonians, Phys. Rev. Lett. **93**, 056402 (2004).

[14] A. Mizel and D. A. Lidar, Three- and four-body interactions in spin-based quantum computers, Phys. Rev. Lett. **92**, 077903 (2004).

[15] G. Savvidy, The gonihedric paradigm extension of the Ising model, Mod. Phys. Lett. B **29**, 1550203 (2015).

[16] P. Dimopoulos, D. Espriu, E. Jané, and A. Prats, Slow dynamics in the three-dimensional gonihedric model, Phys. Rev. E **66**, 056112 (2002).

[17] H. Oike, H. Suwa, Y. Takahashi, and F. Kagawa, Thermally quenched metastable phase in the Ising model with competing interactions, Phys. Rev. B **112**, 064409 (2025).

[18] D. W. Wood and H. P. Griffiths, A self dual relation for an Ising model with triplet interactions, J. Phys. C: Solid State Phys. **5**, L253 (1972).

[19] M. A. Novotny and H. G. Evertz, Computer studies of the Baxter-Wu model: Algorithms, corrections to scaling, and regular impurities, in *Computer Simulation Studies in Condensed-Matter Physics VI*, edited by D. P. Landau, K. K. Mon, and H.-B. Schüttler (Springer, Berlin, 1993), pp. 188–192.

[20] Y. Deng, W. Guo, J. R. Heringa, H. W. J. Blöte, and B. Nienhuis, Phase transitions in self-dual generalizations of the Baxter–Wu model, Nucl. Phys. B **827**, 406 (2010).

[21] I. N. Velonakis and S. S. Martinos, A new cluster algorithm for the Baxter-Wu model, Physica A **390**, 24 (2011).

[22] L. N. Shchur and W. Janke, Critical amplitude ratios of the Baxter–Wu model, Nucl. Phys. B **840**, 491 (2010).

[23] A. A. Saberi, Recent advances in percolation theory and its applications, Phys. Rep. **578**, 1 (2015).

[24] R. A. Myers (ed.), *Encyclopedia of Complexity and Systems Science* (Springer, New York, 2009), Vol. 9.

[25] M. Picco, R. Santachiara, and A. Sicilia, Geometrical properties of parafermionic spin models, J. Stat. Mech. (2009) P04013.

[26] R. J. Baxter and F. Y. Wu, Exact solution of an Ising model with three-spin interactions on a triangular lattice, Phys. Rev. Lett. **31**, 1294 (1973).

[27] R. J. Baxter and F. Y. Wu, Ising model on a triangular lattice with three-spin interactions. I. The eigenvalue equation, Aust. J. Phys. **27**, 357 (1974).

[28] R. J. Baxter and F. Y. Wu, Ising model on a triangular lattice with three-spin interactions. II. Free energy and correlation length, Aust. J. Phys. **27**, 369 (1974).

[29] R. J. Baxter, *Exactly Solved Models in Statistical Mechanics* (Academic Press, London, 1982).

[30] N. Metropolis, A. W. Rosenbluth, M. N. Rosenbluth, A. H. Teller, and E. Teller, Equation of state calculations by fast computing machines, J. Chem. Phys. **21**, 1087 (1953).

[31] D. J. Amit and V. Martin-Mayor, *Field Theory, the Renormalization Group, and Critical Phenomena: Graphs to Computers* (World Scientific, Singapore, 2005).

[32] B. Efron, Bootstrap methods: Another look at the jackknife, in *Breakthroughs in Statistics: Methodology and Distribution*, edited by S. Kotz and N. L. Johnson (Springer, New York, 1992), pp. 569–593.

[33] W. H. Press, S. A. Teukolsky, W. T. Vetterling, and B. P. Flannery, *Numerical Recipes in C* (Cambridge University Press, Cambridge, 1992).

[34] D. Stauffer and A. Aharony, *Introduction to Percolation Theory*, 2nd ed. (Taylor & Francis, London; Bristol, PA, 1994).

[35] M. E. J. Newman and R. M. Ziff, Efficient Monte Carlo algorithm and high-precision results for percolation, Phys. Rev. Lett. **85**, 4104 (2000).

[36] P. H. L. Martins and J. A. Plascak, Percolation on two- and three-dimensional lattices, Phys. Rev. E **67**, 046119 (2003).

[37] M. Akritidis, N. G. Fytas, and M. Weigel, Geometric clusters in the overlap of the Ising model, Phys. Rev. E **108**, 044145 (2023).

[38] W. Janke and A. M. J. Schakel, Fractal structure of spin clusters and domain walls in the two-dimensional Ising model, Phys. Rev. E **71**, 036703 (2005).

[39] M. A. Novotny and D. P. Landau, Critical behavior of the Baxter-Wu model with quenched impurities, Phys. Rev. B **24**, 1468 (1981).

[40] M. L. M. Costa and J. A. Plascak, Monte Carlo study of the spin-1 Baxter-Wu model, Braz. J. Phys. **34**, 419 (2004).

[41] W. Liu, Z. Yan, and Y. Wang, Phase transitions of two spin-1/2 Baxter–Wu layers coupled with Ising-type interactions, Commun. Theor. Phys. **73**, 015602 (2021).

[42] D. Merlini and C. Gruber, Spin-1/2 lattice system: Group structure and duality relation, J. Math. Phys. **13**, 1814 (1972).

[43] A. M. Ferrenberg and R. H. Swendsen, New Monte Carlo technique for studying phase transitions, Phys. Rev. Lett. **61**, 2635 (1988).

[44] F. C. Alcaraz and J. C. Xavier, Conformal invariance studies of the Baxter-Wu model and a related site-colouring problem, J. Phys. A: Math. Gen. **30**, L203 (1997).

[45] F. C. Alcaraz and J. C. Xavier, Critical and off-critical studies of the Baxter-Wu model with general toroidal boundary conditions, J. Phys. A: Math. Gen. **32**, 2041 (1999).

[46] M. E. J. Newman and G. T. Barkema, *Monte Carlo Methods in Statistical Physics* (Oxford University Press, Oxford, UK, 1999).

[47] N. Madras and A. D. Sokal, The pivot algorithm: A highly efficient Monte Carlo method for the self-avoiding walk, J. Stat. Phys. **50**, 109 (1988).

[48] A. D. Sokal, Monte Carlo methods in statistical mechanics: Foundations and new algorithms, in Functional Integration Basics and Applications, in *Proceedings of the 1996 NATO Advanced Study Institute in Cargèse*, edited by C. DeWitt-Morette, P. Cartier, and A. Folacci (Plenum Press, New York, 1997), pp. 131–192.

[49] W. Janke, Monte Carlo methods in classical statistical physics, in *Computational Many-Particle Physics*, Lecture Notes in Physics Vol. 739, edited by H. Fehske, R. Schneider, and A. Weiße (Springer, Berlin, 2008), pp. 79–140.

[50] M. Nightingale and H. Blöte, Universal Ising dynamics in two dimensions, Physica A **251**, 211 (1998).

[51] Z. Liu, E. Vatansever, G. T. Barkema, and N. G. Fytas, Critical dynamical behavior of the Ising model, Phys. Rev. E **108**, 034118 (2023).

[52] M. Bisson, A. Vasilopoulos, M. Bernaschi, M. Fatica, N. G. Fytas, I. G.-A. Pemartín, and V. Martín-Mayor, Universal exotic dynamics in critical mesoscopic systems: Simulating the square root of Avogadro's number of spins, Phys. Rev. Res. **7**, 033218 (2025).

[53] X. J. Li and A. D. Sokal, Rigorous lower bound on the dynamic critical exponents of the Swendsen-Wang algorithm, Phys. Rev. Lett. **63**, 827 (1989).

[54] D. A. Dias, J. C. Xavier, and J. A. Plascak, Critical behavior of the spin-1 and spin-3/2 Baxter–Wu model in a crystal field, Phys. Rev. E **95**, 012103 (2017).

[55] L. N. Jorge, L. S. Ferreira, and A. A. Caparica, On the order of the phase transition in the spin-1 Baxter–Wu model, Physica A **542**, 123417 (2020).

[56] A. Vasilopoulos, N. G. Fytas, E. Vatansever, A. Malakis, and M. Weigel, Universality in the two-dimensional dilute Baxter–Wu model, Phys. Rev. E **105**, 054143 (2022).

[57] A. R. S. Macêdo, A. Vasilopoulos, M. Akritidis, J. A. Plascak, N. G. Fytas, and M. Weigel, Two-dimensional dilute Baxter-Wu model: Transition order and universality, Phys. Rev. E **108**, 024140 (2023).

[58] J. Zierenberg, N. G. Fytas, M. Weigel, W. Janke, and A. Malakis, Scaling and universality in the phase diagram of the 2D Blume-Capel model, Eur. Phys. J. Spec. Top. **226**, 789 (2017).

[59] D. A. Johnston and R. P. K. C. Malmini, Gonihedric 3D Ising actions, Phys. Lett. B **378**, 87 (1996).

[60] D. Espriu, M. Baig, D. A. Johnston, and R. P. K. C. Malmini, Evidence for a first-order transition in a plaquette three-dimensional Ising-like action, J. Phys. A: Math. Gen. **30**, 405 (1997).